Tricalcium silicate Ca3SiO5 superstructure analysis: a route towards the structure of the M1 polymorph

Marie-Noëlle de Noirfontaine, Mireille Courtial, Frederic Dunstetter, Gilles Gasecki, Marcel Signes-Frehel

Tricalcium silicate Ca_3SiO_5 superstructure analysis: a route towards the structure of the M_1 polymorph

Marie-Noëlle de Noirfontaine [I, III,*], Mireille Courtial [I, II], Frédéric Dunstetter [I],
Gilles Gasecki [III], Marcel Signes-Frehel [III]

[I] Laboratoire des Solides Irradiés, École Polytechnique- CNRS UMR 7642- CEA, 91128 Palaiseau, France
[II] Université d'Artois, 1230 Rue de l'Université, 62400 Béthune, France
[III] C.T.G.- Italcementi Group, rue des Technodes, 78931 Guerville, France

Keywords: Ca_3SiO_5; Crystal Structure; M1 Alite; Polymorphism; Powder X-Ray Diffraction

Abstract.

In this paper, we present a structural model for the M_1 polymorph of tricalcium silicate Ca_3SiO_5 from Powder X-Ray Diffraction (XRD) data, including weak intensity superstructure Bragg lines. As no single crystal is available, this structural model has been deduced using the structural relationships found between the previously known triclinic and monoclinic M_3 polymorphs.
We find that the better starting set of atomic positions for Rietveld refinement is the triclinic set and not the monoclinic set. A key observation is that the monoclinic M_1 structure is closer to the low temperature triclinic T_3 structure (within the Golovastikov model) than to the higher temperature monoclinic M_3 structure.
The unit cell and the set of atomic positions of the two best models, called 3<M>*Pc* and 3<T>*Pn* models, are provided. We prefer the 3<M>*Pc* model for it better reproduces the weak characteristic Bragg lines of the superstructure.

Introduction

Anhydrous Portland cement is essentially composed of a synthetic rock named clinker, which contains at least four major phases: two calcium silicates called alite and belite, an aluminate phase and a ferrite phase, and minor phases depending on conditions. During the hydration of cement, the two silicates react with water to produce an ill-crystallised compound (C-S-H), which is responsible for the cohesive properties of hydrated cements, and crystals of portlandite. The same stands for aluminates, except that all the final compounds are crystallized.
Alite is the major constituent of the clinkers, in a concentration ranging from 40 to 70%: it is a solid solution of tricalcium silicate Ca_3SiO_5 with various impurities which presents a complex phase diagram still not well known. Ca_3SiO_5 is called C_3S with the oxide notations (C = CaO, S = SiO_2).
Pure C_3S exhibits six polymorphs from room temperature up to 1100°C [1]: three triclinic forms (T_1, T_2, T_3), two monoclinic forms (M_1 and M_2) and one rhombohedral (R). At room temperature, impurities stabilise some of the high temperature forms of the pure compound, or another monoclinic phase called M_3 alite [2,3]. A list of crystallographic data of the seven polymorphs is given in Table 1.

pure: $T_1 \xleftrightarrow{620°C} T_2 \xleftrightarrow{920°C} T_3 \xleftrightarrow{980°C} M_1 \xleftrightarrow{990°C} M_2 \xleftrightarrow{1070°C} R$

doped (mainly Zn or Mg): $M_1 \xleftrightarrow{990°C} M_2 \xleftrightarrow{1060°C} M_3 \xleftrightarrow{1070°C} R$

In industrial clinkers, M_1 and M_3 polymorphs are the most frequently stabilised phases. The only single crystal structures available in the literature are those of a triclinic polymorph and the M_3 and R polymorphs.

The first single crystal study on C_3S has been proposed by Jeffery [4] who determined an average rhombohedral pseudo structure (*R*3*m* space group) for the triclinic, M_3 and R polymorphs.

[*] Corresponding author. Tel.: +33 1 69 33 44 83; fax: +33 1 69 33 45 54
e-mail address: marie-noelle.de-noirfontaine@polytechnique.edu

In the late 1960's, Guinier, Regourd and co-workers studied the polymorphism of C_3S by powder X-Ray diffraction [1] and this remains the only systematic report. Their analysis of cell parameters in relation to temperature is consistent with displacive transformations [5,6]. The cell deformations have been discussed by the authors in the two characteristic planes of the structure, the monoclinic and the hexagonal plane. However, atomic positions and space groups were not available.
In 1975, Golovastikov *et al.* [7] were able to solve a triclinic structure with a Weissenberg experiment. In the 1980's, the M_3 and R structures have been solved thanks to single crystal studies with a 4-circle diffractometer: the R structure was solved by Nishi & Takéuchi [8] and quasi simultaneously by Il'inets *et al.* [9,10]; the M_3 structure was solved by Nishi & Takéuchi [11]. These structures are characterised by large unit cells, with very many atoms (228 atoms in the reduced unit cell of M_3). Atoms distributed over two positions and complicated orientational disorder of the SiO_4 groups were found in the high temperature phases. A smaller unit cell with average structure referred to as <M> was also proposed for the M_3 polymorph. In 1995, Mumme [12] determined the crystal structure of an alite single crystal extracted from a clinker: the <M> unit cell was identified again, quite similar to that of Nishi, but now as the genuine structure.
During the 1990's, Rietveld's analysis became a powerful tool for powder diffraction data, starting from the atomic models determined by the previous single crystal experiments. In 1997, Berliner *et al.* [13] proposed simplified models of the M_3 polymorph without atoms at split positions, refined on neutron and synchrotron powder diffraction data. De la Torre *et al.* [14] investigated the M_3 polymorph using synchrotron X-Ray and neutron powder data; with the models of Berliner *et al.* [13] and Nishi & Takéuchi [11] as starting models for Rietveld refinement, they provided another superstructure model for M_3, better than the Berliner one.
In 2004, Peterson *et al.* [15,16] used the Golovastikov model of triclinic alite as an average starting model for Rietveld refinement with synchrotron powder diffraction data of the three triclinic polymorphs. They found superstructure Bragg lines in the T_1 and T_2 polymorphs, with decreasing intensity passing from T_1 to T_2. As yet, no set of atomic positions for the real superstructures in T_1 and T_2 polymorphs is known: average models of Golovastikov-type are provided. The Golovastikov model can be used for T_3 alite and as an averaged model for T_1 and T_2 alite. Finally, the Golovastikov model was again found appropriate for the T_3 polymorph by De la Torre *et al.* [17], who used synchrotron data of T_1 and T_3 polymorphs. Their T_3 model was validated for Rietveld quantitative analysis on laboratory Portland clinkers with less than 1% of MgO impurity. Guinier, Regourd and co-workers [1] already mentioned the appearance of such superstructure Bragg lines for the lower temperature triclinic polymorphs. In this paper, we label the Golovastikov model as the "T model".

In a series of papers [18-21] we have proposed an extensive analysis of the polymorphism of tricalcium silicate, based on the superstructure relationships between the known structures, together with powder X-ray diffraction data analysis of synthetic alites M_1 and M_3 compared to M_1 and M_3-based industrial clinkers. Only averaged models were discussed in [19]. It is the aim of the present paper to present non-averaged models for the M_1 polymorph and give the set of atomic positions.

The paper is organised as follows. The first section briefly describes the synthesis of the M_1 polymorph samples and the collection of powder X-Ray diffraction (XRD) data. The second section is devoted to the construction of the starting atomic models needed for Rietveld refinement with our data. The last section presents the data analysis of the XRD data.

1. Experimental

Pure C_3S (in the triclinic form) and two alites, M_1 and M_3[1], were synthesised at C.T.G. Laboratory (Italcementi Group). The formulation for M_1 is based on the data of Qing *et al.* [22]. As was already observed by Maki & Goto [23], sulphate impurities stabilise the M_1 form and magnesium impurities stabilise the M_3 form. The proportion (wt %) of the different impurities added to pure C_3S to synthesise the M_1 form is the following: 93.13 % C_3S + 0.96 % Al_2O_3 + 0.96 % MgO + 0.96 % Fe_2O_3 + 4 % $CaSO_4$. The M_3 alite was synthesised from a mixture of $CaCO_3$, SiO_2, MgO, Al_2O_3 in the stoechiometric proportion $Ca_{2.879}Si_{0.971}Mg_{0.112}Al_{0.0439}O_5$.

These compounds were analysed by X-Ray fluorescence and X-Ray powder diffraction. Using the usual stoechiometric oxide notations, the post-synthesis chemical analysis of the M_1 alite is the following (wt%): CaO: 70.48%, SiO_2: 24.47%, SO_3: 1.55%, Al_2O_3: 1.05%, Fe_2O_3: 1.05%, MgO: 0.99%, (Ignition loss: 0.41%).

Powder XRD data were collected in the 2θ range 10-90°, step interval 0.02°, with a Philips PW 1050/70 diffractometer using CuKα radiation. The diffraction patterns are discussed in the last section.

[1] The synthetic M_3 alite is used here as a tool to confirm the validity of the averaging process of the atomic positions described in §2.3.

2. Superstructure analysis as a tool to build starting atomic positions

No atomic position is known for the M_1 polymorph. In absence of single crystal data, some preliminary atomic model is needed to refine the models using powder diffraction data. A possible way is to extract a set of atomic positions from the available information on the other polymorphs and their mutual relationships.

In the phase diagram of doped C_3S, the M_1 polymorph occupies an intermediate position between the low temperature triclinic polymorphs (T_1, T_2, T_3) and the high temperature (M_2, M_3) polymorphs. Among these neighbouring polymorphs, the only known atomic models were triclinic and M_3 models. Therefore, in the following, we consider the triclinic and M_3 polymorphs as the closest known reference points.

Guinier, Regourd & coworkers [5,6] have shown that the transformations between the polymorphs are displacive transformations with a progressive deformation of the unit cell, especially the angles. Therefore, any atomic model for the M_1 polymorph is supposed to be intermediate between the known atomic models of the triclinic and M_3 polymorphs. However, the volumes of the unit cells of the three polymorphs T_1, M_1 and M_3 are rather different due to various superstructure relations with respect to the underlying trigonal translational symmetry of the pattern. No direct link was found. However, an indirect link exists.

2.1. Relations between the unit cells of the various polymorphs

The first step is to find the coordinate transformation relationships between the three polymorphs.

We have shown [18,20] that introducing two elementary pseudo-monoclinic blocks of same volume named <M> and <T> provides the expected links between the three polymorphs. The pseudo-monoclinic unit cells <M> and <T> are equivalent; the various published unit cells (including the unit cells discussed in this paper) and their mutual relationships are summarised in the flowchart of Fig. 1 and Table 2.

(i) Unconventional unit cells are necessary for the structural relationships to become apparent. In Fig. 1 and Table 2, M'_1 and M'_3 are unconventional unit cells respectively equivalent to the M_1 and M_3 conventional monoclinic unit cells of references [1,11].

(ii) The G triclinic published unit cell [7] of the T polymorph exhibits no easy relationship with the other unit cells since none of its basis vectors lies in the hexagonal or monoclinic planes. Using the transformation matrix

$$\left[\mathbf{a}_{G'}, \mathbf{b}_{G'}, \mathbf{c}_{G'}\right] = \left[\mathbf{a}_{G}, \mathbf{b}_{G}, \mathbf{c}_{G}\right] \begin{bmatrix} 1 & 0 & 1 \\ 1 & 1 & 0 \\ 0 & 0 & 1 \end{bmatrix}$$

one finds another triclinic unit cell G' with basis vectors $\mathbf{a}_{G'}$ and $\mathbf{c}_{G'}$ now lying in the monoclinic plane; moreover, $\mathbf{b}_{G'}=2\mathbf{a}_H$, where $\mathbf{a}_H$ is the hexagonal vector (Fig. 2a).
The cell transformation G' $\rightarrow$ 3G'$^{(1)}$

$$\left[\mathbf{a}_{3G'^{(1)}}, \mathbf{b}_{3G'^{(1)}}, \mathbf{c}_{3G'^{(1)}}\right] = \left[\mathbf{a}_{G'}, \mathbf{b}_{G'}, \mathbf{c}_{G'}\right] \begin{bmatrix} 1 & -2 & 0 \\ 0 & 3 & 0 \\ 0 & 1 & 1 \end{bmatrix}$$

leads to a tripled cell with a cell centring described by the centring vectors (0,0,0); (2/3,1/3,2/3); (1/3,2/3,1/3). The 3G'$^{(1)}$ unit cell is pseudo-monoclinic. Among the various equivalent pseudo monoclinic unit cells of 3G'$^{(1)}$, the only important one is the 3G' unit cell[2] defined by the cell transformation G' $\rightarrow$ 3G'

[2] The unit cell transformation G' $\rightarrow$ 3G'$^{(2)}$ $\rightarrow$ 3G' is defined as follows:
- 3G'$^{(1)}$ $\rightarrow$ 3G'$^{(2)}$ is the standard transformation between choices 1 and 2 of the pseudo monoclinic unit cells,
- 3G'$^{(2)}$ $\rightarrow$ 3G' reverts the **a** and **c** axes of the 3G'$^{(2)}$ unit cell.

$$\left[\mathbf{a}_{3G'}, \mathbf{b}_{3G'}, \mathbf{c}_{3G'}\right] = \left[\mathbf{a}_{G'}, \mathbf{b}_{G'}, \mathbf{c}_{G'}\right] \begin{bmatrix} 1 & -2 & -1 \\ 0 & 3 & 0 \\ 1 & 1 & 0 \end{bmatrix}$$

with the centring vectors (0,0,0); (2/3,1/3,0); (1/3,2/3,0).
These various unit cells are listed in the upper part of Table 2.

(iii) The equivalence (Fig. 2b) between the two <M> and <T> blocks (related to choices 1 and 3 respectively in monoclinic symmetry) and the cell transformation <T> $\rightarrow$ <M>

$$\left[\mathbf{a}_{<M>}, \mathbf{b}_{<M>}, \mathbf{c}_{<M>}\right] = \left[\mathbf{a}_{<T>}, \mathbf{b}_{<T>}, \mathbf{c}_{<T>}\right] \begin{bmatrix} 1 & 0 & 1 \\ 0 & 1 & 0 \\ 0 & 0 & 1 \end{bmatrix}$$

provide the relationships for transformation of atomic coordinates, derived from the relationships between the unit cells, namely (Fig. 3):

$M'_1 \equiv 3\ <M> \equiv\ (3,1,1)\ <M>$
$M'_3 \equiv 6\ <M> \equiv\ (2,1,3)\ <M>$
$3G' \equiv 9\ <T> \equiv\ (3,3,1)\ <T>$

where the notation n<M>, n=pqr, stands for (p,q,r)<M> as a condensed notation for a (p $\mathbf{a}_{<M>}$, q $\mathbf{b}_{<M>}$, r $\mathbf{c}_{<M>}$) supercell of <M>. In the following a set of integers - n or (p,q,r) - is used to label the volume of the unit cell considered as a multiple of the two possible elementary blocks.

2.2. Atomic positions versus symmetry elements

The next step is to find the space groups to be considered in the data refinement.

Let us consider the various available monoclinic space groups.

As in ref. [20], models are labelled by combining the shape (and/or the volume of the unit cell) and the space group type used to generate the atomic positions. For example, 3<T> $P\bar{1}$ labels a unit cell with a volume triple of that of the <T> elementary block and a space group $P\bar{1}$.

Due to the fact that the average pseudo-symmetry is described within the space group *R*3*m* (and not $R\bar{3}m$), only symmetry operations belonging to this space group can be used in future discussion. This means explicitly that neither inversion centre nor two-fold axes are eligible for testing. The existence of a *2* axis would induce the equivalence between the silicate ions: this was already rejected with the first work of Jeffery [4] and has also been discussed by Il'inets *et al.* [9]. The *R3m* group being a polar space group, a free z parameter is allowed for any atom lying along the axis, giving a higher flexibility of the structure without drastic symmetry change.

The only remaining space groups are *Pm*, *Pc*, *Cm* and *Cc*.

To go further, one needs to take into account
(i) the experimental results of a triple periodicity along the rhombohedral axis $\mathbf{a_R} \equiv \mathbf{a_{<M>}} \equiv \mathbf{a_{<T>}}$ observed by TEM (Fig. 4),
(ii) the atomic positions. Fig. 5 shows the skeleton of the SiO_4 groups, more extensively discussed in ref. [18]. One can observe (Fig. 6) a stacking of two types of monoclinic planes: planes of calcium and silicon ions located at y_{Si} and $y_{Si}+1/2$ referred to as mixed planes, separated by planes of calcium ions only, located at $y_{Si}+1/4$, $y_{Si}+3/4$. In the mixed planes, one observes herringbone-like chains of ions, with axial Si_1 ions and lateral Si_2 and Si_3 ions, separated by parallel and similar herringbone-like chains of calcium ions for which the discussion is identical.

The action of the pseudo-hexagonal symmetry is to relate parallel herringbones of adjacent mixed planes by the $\mathbf{a_H}$ or $\mathbf{b_H}$ hexagonal basis vectors. In *R*3*m* and its monoclinic subgroups, these average hexagonal translations are performed

by true translation or glide vectors in the rhombohedral and monoclinic space groups respectively; they are performed by the inversions in the $P\bar{1}$ triclinic space group. More precisely, the Si_2 and Si_3 ions located on each side of the herringbones are related to other ions, Si'_2 and Si'_3, located on the sides of chains that belong to the neighbouring planes of the same families, located at y =+/-1/2. Always within an average view of the problem, all the calcium planes are related by a pseudo-translation **b**/2 where **b** is the monoclinic axis of the elementary block. On the other hand, the mixed planes exhibit a periodicity **b** along the monoclinic axis. This double periodicity is not compatible with any space group and any superstructure of the three possible elementary blocks.

The *Cc* group has two glide mirrors, axial and diagonal glide planes **c** and **n**. The diagonal glide plane **n** (x+1/2,-y+1/2, z+1/2) makes it necessary to double the unit cell along the **a** direction to be consistent with the atomic positions in the mixed planes. Inasmuch as a tripling of the unit cell is observed experimentally (Fig. 4), the *Cc* group must be rejected. The *Pm*, *Pc* and *Cm* space groups have either a mirror (*Pm*), a glide mirror (*Pc*) or both (*Cm*). In order to achieve the **b** pseudo-periodicity of the mixed Si-Ca planes, the *m* mirror must be in the Si-Ca plane. Likewise, the glide mirrors must be located in the calcium planes in order to be consistent with the **b**/2 pseudo-periodicity (Fig. 6).

Finally, three space group types are left: *Pm*, *Pc*, *Cm*. The tested models are the following:

3<T>*Pn*, 3<T>*Pm*, 3<T>*Im*
3<M>*Pc*, 3<M>*Pm*, 3<M>*Am*

where the integer 3 is always related to the basis vector **a**.

The last step is to find the list of starting atomic positions for each of these six models.

2.3. Building a starting atomic model

2.3.1. Averaging the literature data for the triclinic and M_3 polymorphs

Using the structural relationships, one can build various averaged atomic models derived either from the triclinic polymorph or from the M_3 polymorph. To distinguish the origin of the averaged atomic positions, let us give – for the time being – the index T, Nishi or Mumme to a model derived from triclinic or M_3 published data.

A $3\langle T\rangle_T$ set of atomic positions can be derived directly by averaging the $9\langle T\rangle_T$ set of atomic positions for the triclinic polymorph as follows. The Golovastikov structure G [7] is transformed into a 3G' ≡ 9<T> [18,20] set of atomic parameters using the transformation matrix P = 2, -1, -1; 1, 1, -1; 1, 1, 0 and the centring vectors given in § 2.1. Then, two average structures $3\langle T\rangle_T$ and $\langle T\rangle_T$ are derived, validated on our triclinic samples powder data. The averaging procedure takes all the 486 atomic positions (i.e. the *P1* space group) into account. The averaged positions are found to be compatible with the $P\bar{1}$ space group. Therefore, the two models $3\langle T\rangle_T$ and $\langle T\rangle_T$ arising from the triclinic data are referred to as $3\langle T\rangle P\bar{1}$ and $\langle T\rangle P\bar{1}$.

No 3<M> set of atomic positions can be built by a simple averaging of a known structure, for the longest vector **a** is found in the 6<M> structure, with $\mathbf{a}_{6\langle M\rangle}=2\mathbf{a}_{\langle M\rangle}$. It is necessary to go through a smaller <M> averaged set of atomic positions. Starting from the M_3 polymorph, we used either the Mumme published structure [12] $\langle M\rangle_{Mumme}$ *Am* or an averaged structure $\langle M\rangle_{Nishi}$ *Am* derived from the published Nishi & Takéuchi data [11]. These models were validated on our M_3 samples powder XRD data. Starting from the triclinic polymorph, we use the $\langle T\rangle_T$ model and the equivalence[3] between the <M> and <T> pseudo-monoclinic unit cells to build a $\langle M\rangle_T$ set of atomic positions. Then several 3<M> starting atomic models ($3\langle M\rangle_{Mumme}$, $3\langle M\rangle_{Nishi}$ and $3\langle M\rangle_T$) are built by concatenation of three identical <M> sets.

2.3.2. Starting model consistent with the monoclinic symmetry of the M_1 polymorph

a) Starting from M_3 data

The averaged atomic models derived from the M_3 polymorph can be directly used to refine the M_1 polymorph data, with minor modifications intended to adapt the atomic positions to the symmetry elements of each space group.

[3] $\langle T\rangle P\bar{1}$ and $\langle M\rangle P\bar{1}$ triclinic structures are fully equivalent, due to the conservation of the inversion centres: $\langle M\rangle P\bar{1} \equiv \langle T\rangle P\bar{1}$. Things are changing in the case of supercells $n\langle M\rangle P\bar{1}$ or $n\langle T\rangle P\bar{1}$, with n>1.

b) Starting from triclinic data

The problem is to introduce a monoclinic symmetry in the set of triclinic atomic positions 3<T>$P\bar{1}$. Tables 3 & 4 illustrate the situation of the SiO_4 groups for the simplest case <T>$P\bar{1}$; although less simple rational coordinates, the same situation is found in the 3<T>$P\bar{1}$ case. In the <T> unit cell, Si and Ca ions are close to rational coordinates. Transforming these rational coordinates from <T> to <M> leads to other rational coordinates in the <M> unit cell (Table 3 & Fig. 5). Table 4 shows the exchange between the symmetry-related Si2 and Si3 ions. In the <M>$P\bar{1}$ symmetry, Si2 and Si2' are related by an inversion centre, and the same situation occurs for Si3 and Si3'. In the <M>*P*c symmetry, Si2 and Si3' on one side, Si3 and Si2' on the other side are now related by the glide mirror *c*. A similar behaviour is found for the calcium ions.

The same situation stands for 3<T>*Pn*, made easier since no <T>-<M> transformation is needed.

The 3<M>*Pm* and 3<M>*Am* starting models were derived from the 3<M>*P*c model.

3. Data analysis of the M_1 data

3.1. Method

The different models have been refined using Rietveld analysis. The two packages FullProf [24] and GSAS [25] were used. In each refinement, a pseudo-Voigt profile shape function was considered and the SiO_4 tetrahedra were treated as rigid bodies, with d_{Si-O} = 1.62 Å. The refined parameters were the scale factor, the instrumental parameters (angular offsets, background, peak half-width parameters), the cell parameters, the atomic positions and a common Debye-Waller factor U_{iso} = 0.025 $Å^2$.
The agreement factors discussed in the following are the R_B (R-Bragg) and R_F (R-factor) given by the FullProf program. It is important to underline that an analysis of the agreement factors alone is not sufficient to choose among the models. A visual control of the reproduction of the small diffraction lines characteristic of the superstructures is absolutely necessary. This method was validated and controlled on our data for triclinic, M_1 and M_3 compounds [21].

3.2. Results

Among the six models tested (Table 5), the best refinements were obtained with the 3<M>*Pc* and 3<T>*Pn* models. The atomic positions for these two best models are given in Tables 6 & 7.
The change of glide to mirror (*Pm* or *Cm* space groups) always decreases the quality of the refinement: (i) the position of the calculated diffraction lines is not compatible with the position of the observed lines, and (ii) the best refinement with these space groups is the one with the orientational disorder closest to that of the 3<M>*Pc* model. For these reasons, we reject the *Pm* and *Cm* space groups.
It is interesting to note that the orientational disorder of the SiO_4 tetrahedra of the best 3<M>*Pc* model is already very close to the orientational disorder described by Nishi & Takéuchi [11] in the M_3 polymorph, which shows that the distinction between the M_1 and M_3 orientational disorder is more closely related to the presence of the mirror than to the very detail of the orientational disorder itself.

As far as the agreement factors are rather similar and the diffraction pattern is equally well reproduced by both models, the distinction between the 3<M>*Pc* and 3<T>*Pn* models is more difficult. The two calculated diffraction patterns are sketched on Fig. 7. A systematic discrepancy is observed for the line 900, due to textural effects observed in almost all the samples of all the polymorphs, especially in industrial clinkers. A visual comparison of the experimental and calculated diffraction patterns (Fig. 7) shows that the small superstructure diffraction line observed at $2\theta_{Cu}$=25.45° as the second line of a doublet is systematically better reproduced by the 3<M>*Pc* model than by the 3<T>*Pn* model for all our samples. Therefore, we finally choose the 3<M>*Pc* model as the best model, but the other one cannot be definitely rejected.

3.3. Discussion

The Golovastikov model can be considered as a good starting model for T_3 data refinement, whereas the true structure of the T_1 polymorph is in fact a superstructure of the structure described by the Golovastikov model. These results are

not in contradiction with our approach but, on the contrary, they improve our argument, for we can reasonably consider that our triclinic averaged models are close to a T_3 model.

Therefore, we can conclude that concerning the atomic positions, the M_1 structure is close to the T_3 structure. The inversion centres of the triclinic structure are replaced by glide mirrors in the monoclinic structure, with only a slight effect on isolated atoms. The main effect of this change of symmetry concerns the SiO_4 tetrahedra, which already exhibit in the M_1 polymorph the trends of the disorder found in the M_3 polymorph.

Conclusion

Using the superstructure relationships between the polymorphs of tricalcium silicate, a structural model is proposed in this paper, as a first attempt to handle the M_1 polymorph. The rhombohedral translation $\mathbf{a}_R$ of the the trigonal underlying symmetry is related to the glide mirrors in the *Cm* symmetry of the M_3 polymorph and to the inversions in the triclinic symmetry. The two monoclinic polymorphs M_1 and M_3 are two distinct superstructures of the same <M> block and the triclinic polymorph is a superstructure of the <T> block. The equivalence between the two <M> and <T> blocks (respectively choice 1 and choice 3 in pseudo-monoclinic symmetry) provides the relationships for transformation of atomic coordinates.

Starting from the published single crystal data of the triclinic and monoclinic M_3 polymorphs, we derive various starting sets of atomic positions for the subsequent Rietveld analysis of powder X-Ray diffraction data. Six models are tested, consistent with (i) the multiplicity 3 along the monoclinic axis $\mathbf{a}_{M1}$ and (ii) the trigonal underlying pseudo-translational symmetry of the pattern.

The final atomic model is found to be closer to the atomic positions of the Golovastikov model, which describes the structure of the T_3 polymorph located just below the M_1 polymorph in the phase diagram of tricalcium silicate, than to those of the M_3 polymorph, except for the orientational disorder which already prefigures the disorder of the M_3 polymorph.

Concerning the data analysis, the important point is that the two best models, 3<M>*Pc* and 3<T>*Pn,* only differ in one superstructure Bragg line: the crystallographic residues are rather similar and a specific inspection of the $2\theta_{Cu}$=24.5-26° is needed in order to clearly identify the M_1 polymorph. However, on the basis of our data we prefer the 3<M>*Pc* model.

Acknowledgements

The authors would like to thank M. Pierre Jaugey (Ciments CALCIA, France) and Prof. Hélène Zanni for their constant support of this work, Prof. Micheline Moranville for many valuable discussions, Prof. Henri Szwarc for a critical reading of the manuscript, and Dr Spencer Brown for his kind linguistic assistance. The authors dedicate this paper to Gerard Jaskierowicz (deceased) for his enthusiastic collaboration for the TEM experiments.

References

[1] M. Bigare, A. Guinier, C. Mazieres, M. Regourd, N. Yannaquis, W. Eysel, T. Hahn, E. Woermann, Polymorphism of tricalcium silicate and its solid solutions, *Journal of the American Ceramic Society*. **1967**, *50(11)*, 609.
[2] I. Maki, S. Chromy, Microscopic study on the polymorphism of Ca_3SiO_5, *Cement and Concrete Research*. **1978**, *8(4)*, 407.
[3] M. Regourd, Polymorphisme du silicate tricalcique. Nouvelles données de la diffraction des rayons X, *Comptes rendus de l'Académie des Sciences de Paris*. **1979**, *289(B)*, 17.
[4] J.W. Jeffery, The crystal structure of tricalcium silicate, *Acta Crystallographica*. **1952**, *5*, 26.
[5] A. Guinier, M. Regourd: Structure of Portland cement minerals; pp. 1 in *Proceedings of the 5th International Symposium on the Chemistry of Cement*. Tokyo, 1968.
[6] M. Regourd, Cristallographie des constituants du clinker de ciment Portland, *Bulletin de Liaison-Laboratoires Routiers*. **1970**, *N° spécial 0*, 58.
[7] N.I. Golovastikov, R.G. Matveeva, N.V. Belov, Crystal structure of the tricalcium silicate $3CaO.SiO_2 = C_3S$, *Soviet Physics Crystallography*. **1975**, *20(4)*, 441.
[8] F. Nishi, Y. Takéuchi, The rhombohedral structure of tricalcium silicate at 1200°C, *Zeitschrift für Kristallographie*. **1984**, *168*, 197.
[9] A.M. Il'inets, Y.A. Malinovskii, N.N. Nevskii, Crystal structure of the rhombohedral modification of tricalcium silicate Ca_3SiO_5, *Soviet Physics Doklady*. **1985**, *30(3)*, 191.
[10] A.M. Il'inets, M.J. Bikbau: New rhombohedral modification Ca_3SiO_5 and mechanism of atomic transformation during the phase transition; pp. 77 in *Proceedings of the XII European Crystallographic Meeting*. Moscow, 1989.
[11] F. Nishi, Y. Takéuchi, Tricalcium silicate $Ca_3O[SiO_4]$: the monoclinic superstructure, *Zeitschrift für Kristallographie*. **1985**, *172*, 297.
[12] W.G. Mumme, Crystal structure of tricalcium silicate from a Portland cement clinker and its application to quantitative XRD analysis, *Neues Jahrbuch für Mineralogie*. **1995**, *4*, 145.
[13] R. Berliner, C. Ball, P.B. West, Neutron powder diffraction investigation of model cement compounds, *Cement and Concrete Research*. **1997**, *27(4)*, 551.
[14] A.G. de la Torre, S. Bruque, J. Campo, M.A.G. Aranda, The superstructure of C_3S from synchrotron and neutron powder diffraction and its role in quantitative phase analyses, *Cement and Concrete Research*. **2002**, *32*, 1347.
[15] V.K. Peterson, A Rietveld refinement investigation of a Mg-stabilized triclinic tricalcium silicate using synchrotron X-ray powder diffraction data, *Powder Diffraction*. **2004**, *19(4)*, 356.
[16] V.K. Peterson, B.A. Hunter, A. Ray, Tricalcium silicate T1 and T2 polymorphic investigations: Rietveld refinement at various temperatures using synchrotron powder diffraction, *Journal of the American Ceramic Society*. **2004**, *87(9)*, 1625.
[17] Á.G. de la Torre, R.N. de Vera, A.J.M. Cuberos, M.A.G. Aranda, Crystal structure of low magnesium-content alite: Application to Rietveld quantitative phase analysis, *Cement and Concrete Research*. **2008**, *38(11)*, 1261.
[18] F. Dunstetter, M.-N. de Noirfontaine, M. Courtial, Polymorphism of tricalcium silicate, the major compound of Portland cement clinker: 1. Structural data: review and unified analysis, *Cement and Concrete Research*. **2006**, *36(1)*, 39.
[19] M.-N. de Noirfontaine, F. Dunstetter, M. Courtial, G. Gasecki, M. Signes-Frehel, Polymorphism of tricalcium silicate, the major compound of Portland cement clinker: 2. Modelling alite for Rietveld analysis, an industrial challenge, *Cement and Concrete Research*. **2006**, *36(1)*, 54.
[20] M.-N. de Noirfontaine, F. Dunstetter, M. Courtial, G. Gasecki, M. Signes-Frehel, Tricalcium Silicate Ca_3SiO_5, the major component of anhydrous Portland Cement: on the conservation of distances and directions and their relationship to the structural elements, *Zeitschrift für Kristallographie*. **2003**, *218(1)*, 8.
[21] M. Courtial, M.-N. de Noirfontaine, F. Dunstetter, G. Gasecki, M. Signes-Frehel, Polymorphism of tricalcium silicate in Portland cement: a fast visual identification of structure and superstructure, *Powder Diffraction*. **2003**, *18(1)*, 7.
[22] Y. Qing, K. Jianmin, L. Baoyuan: Effect of fluorite-gypsum composite mineralizer on the microstructure and properties of Portland cement clinker phase; pp. 342 in *Proceedings of the 9th International Congress on the Chemistry of Cement*. New Delhi, 1992.
[23] I. Maki, K. Goto, Factors influencing the phase constitution of alite in Portland cement clinker, *Cement and Concrete Research*. **1982**, *12(1)*, 301.
[24] J. Rodriguez-Carvajal, Note prepared for the Nordic Research Course. The Rietveld Method in Practice: the Program FullProf. **1994**.
[25] A.C. Larson, R.B. Von Dreele, GSAS General Structure Analysis System, *Operational Manual*. **2000**, 1.

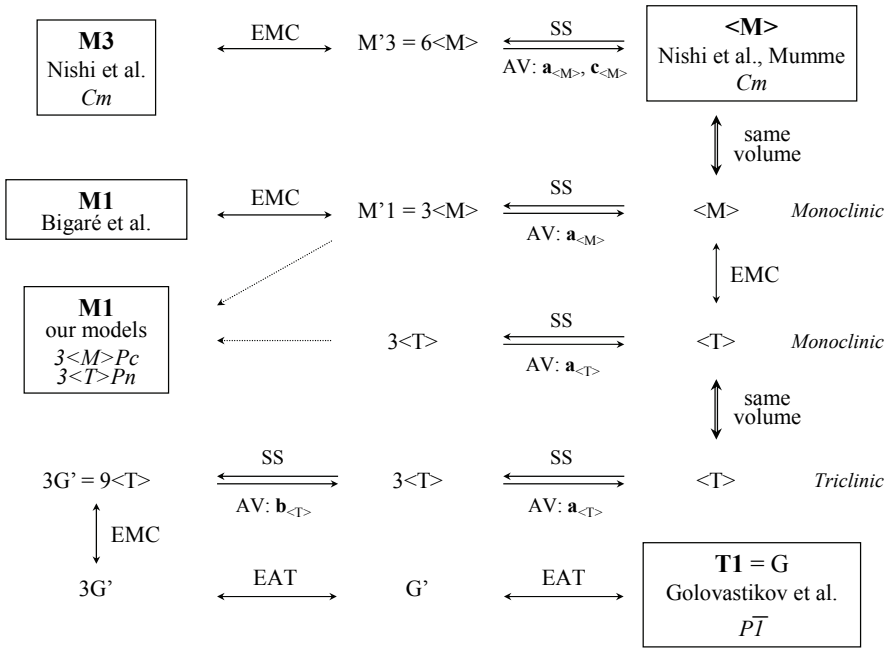

Fig. 1. Flowchart of the superstructure relationships between the unit cells introduced in this paper.
The boxes are related to the published experimental data
EMC Equivalent Monoclinic unit Cell
EAT Equivalent by Axes Transformation and/or use of non-primitive unit cell
SS Superstructure
AV: directions Average along the given direction(s)

The simple arrows are related to the transformations which conserve the content of the unit cell: the models located on each side of such arrows constitute various alternatives to the production of the same diffraction pattern.


The double arrows are related to a modification of the unit cell content: the models located on each side of such arrows produce distinct diffraction patterns due either to different volumes, different symmetry elements or different atomic positions.

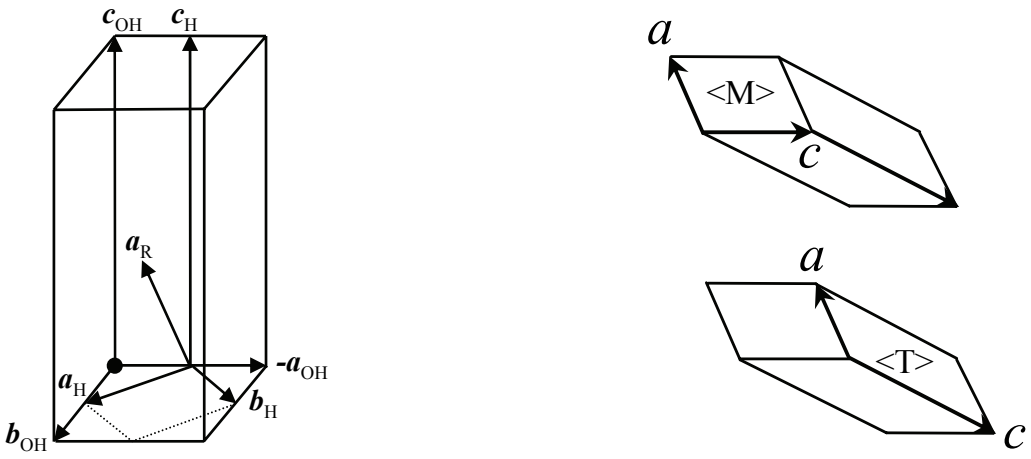

Fig. 2. Unit cells related to the various symmetries or pseudo-symmetries

a) Unit cell vectors associated to the pseudo-rhombohedral symmetry: rhombohedral R, hexagonal H and orthohexagonal OH unit cells. $V_{OH}=2V_H$; $V_H=3V_R$.

b) Average triclinic <T> unit cell, related to the <M> and rhombohedral unit cell

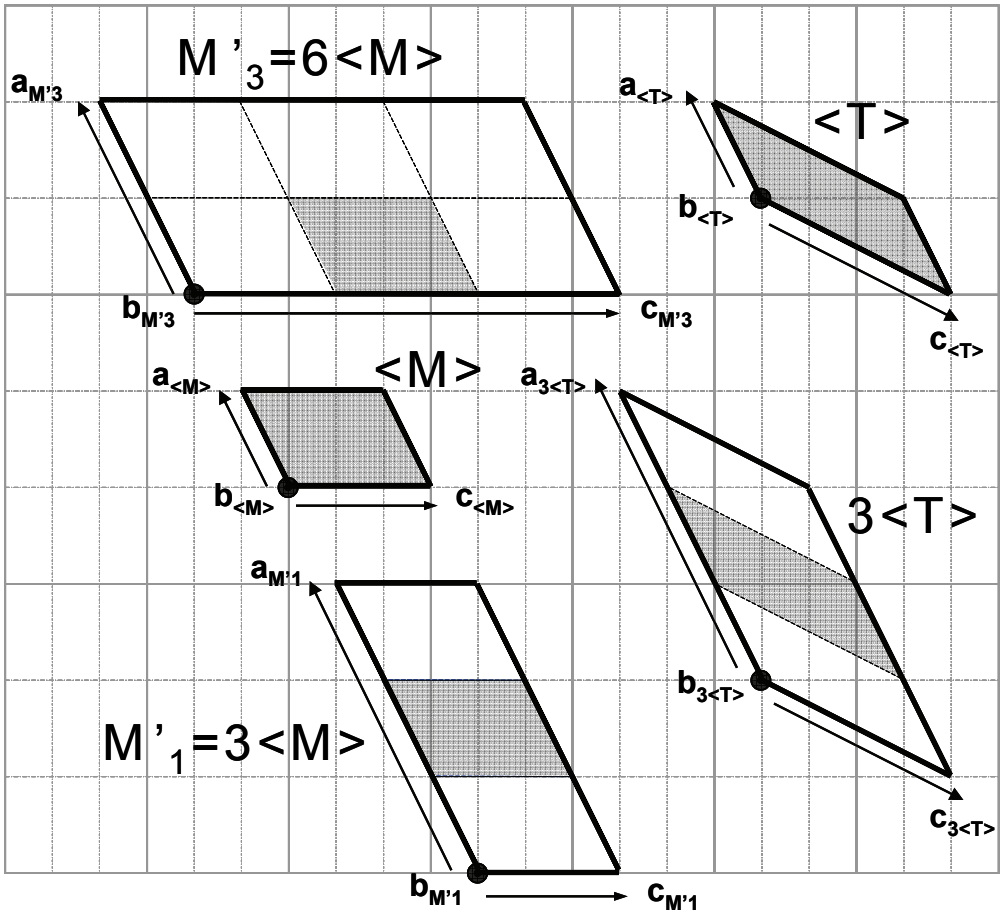

Fig. 3. Unconventional unit cells used in the flowchart of Fig. 1. The unit cell 3G' ≡ 9 <T> ≡ (3,3,1) <T> discussed in § 2.1 is a supercell of the 3<T> unit cell, with $\mathbf{a}_{3G'} = \mathbf{a}_{3<T>}$, $\mathbf{b}_{3G'} = 3\mathbf{b}_{3<T>}$, $\mathbf{c}_{3G'} = \mathbf{c}_{3<T>}$. The primitive unit cell G' - given as an alternative unit cell for the Golovastikov unit cell G - is given by $\mathbf{a}_{G'} = -\mathbf{c}_{3<T>}$, $\mathbf{b}_{G'} = \mathbf{b}_{<M>} - \mathbf{c}_{<M>}$, $\mathbf{c}_{G'} = \mathbf{a}_{3<T>} + \mathbf{c}_{3<T>}$.

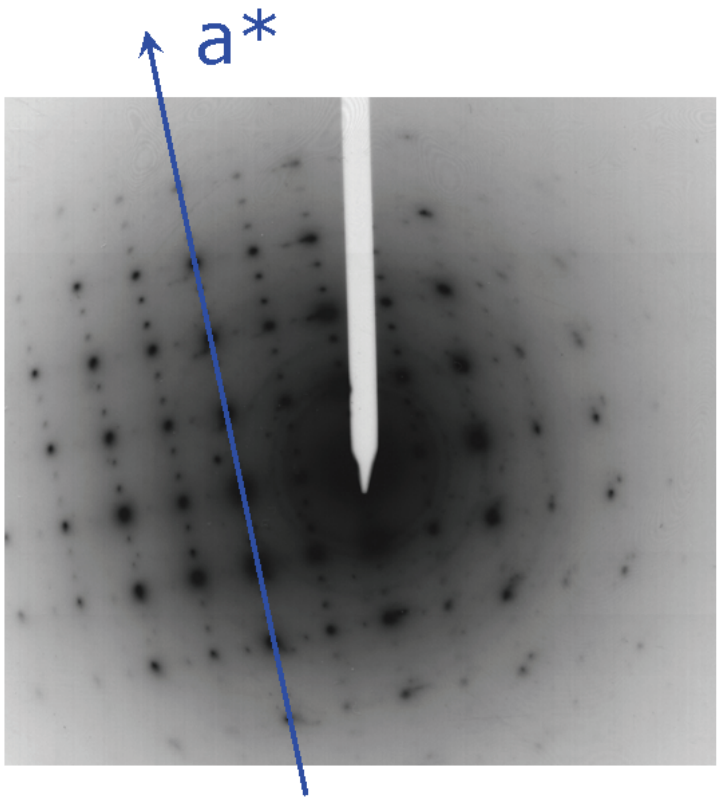

Fig. 4 TEM diffraction pattern of M_1 alite. Philips CM30 300KV (Laboratoire des Solides Irradiés). The polycrystalline sample was distributed on a carbon grid and the mono-crystalline grains were oriented with respect to the electron beam using sample holder rotations.

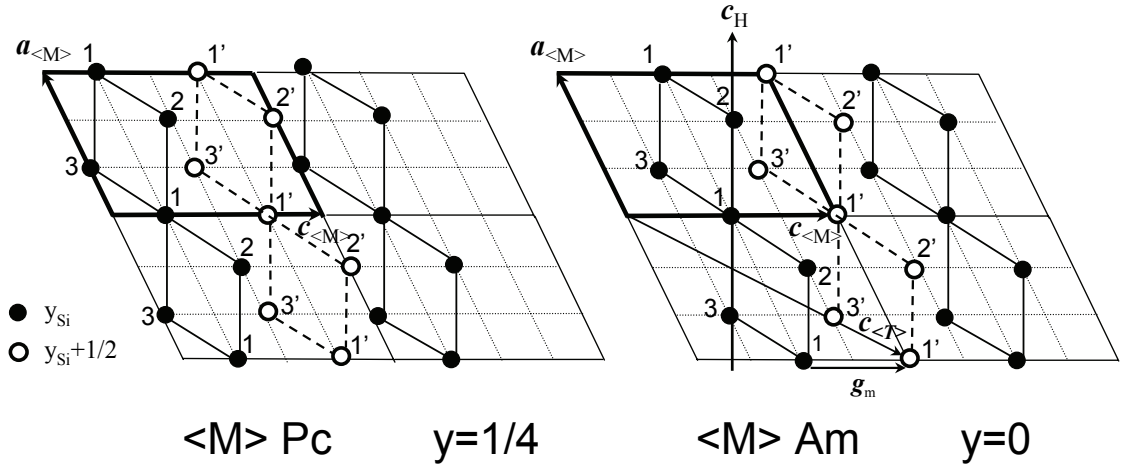

Fig. 5. The herringbones-like chains of silicate ions Si_1, Si_2 and Si_3. These chains are separated by the hexagonal vectors $\mathbf{a}_H$ or $\mathbf{b}_H$ relating a plane y_{Si} and a plane y_{Si}+/- ½. $\mathbf{g}_m$ is the projection of $\mathbf{b}_H$ onto the monoclinic plane.

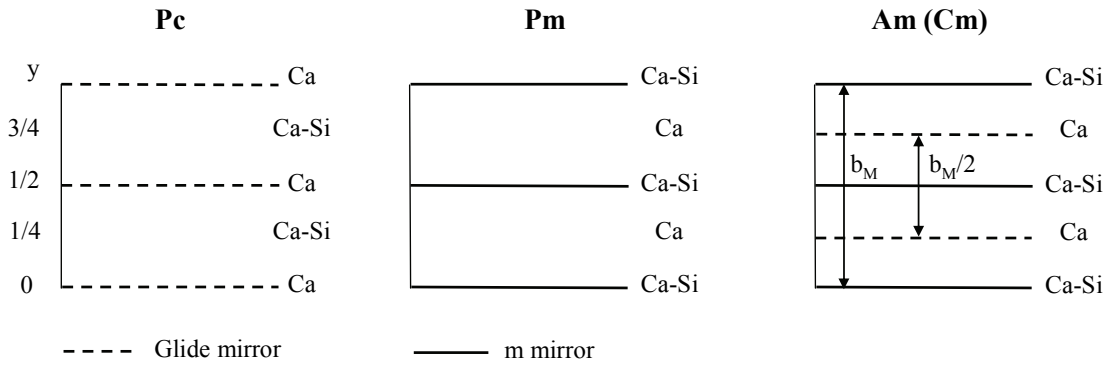

Fig. 6. Relations between the symmetry elements in the *Pc*, *Pm*, *Cm* space groups and the chemical content of monoclinic planes of the structure.

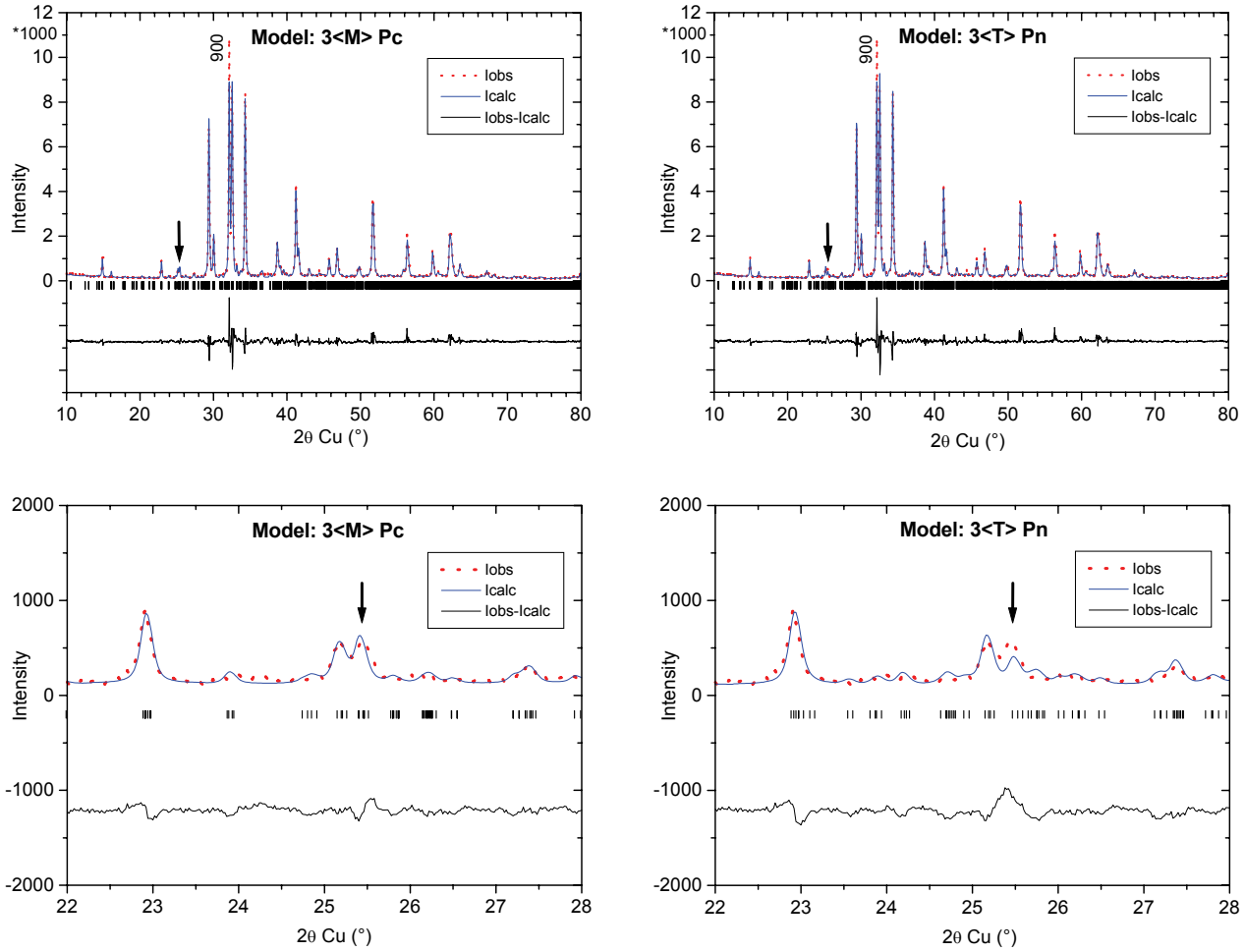

Fig. 7. Rietveld refinements of a powder diffraction pattern of M_1 alite with the structural models 3<M> *Pc* and 3<T> *Pn* proposed in this paper. The 3<M> *Pc* superstructure is necessary to index and reproduce all the lines of the diagram, especially the second line of the doublet in the 24.8-25.8° $2\theta_{Cu}$ range, which is a characteristic superstructure line, related to the angular window W1 introduced in Fig. 2 of ref. [21].

Table 1. Crystallographic data of the seven polymorphs known for tricalcium silicate;
(pOH) = pseudo-orthohexagonal symmetry;
SC = single crystal datal. PWD = powder diffraction data. SR = synchrotron radiation data.
The column "xyz" indicates whether xyz data are provided or not in the given reference.

Polymorph	Symmetry group	Type of data	a (Å)	b (Å)	c (Å)	α (°)	β (°)	γ (°)	xyz in ref.	Reference
R	*R3m*	SC SC	7.135 7.0567	7.135 7.0567	25.586 24.974	90	90	120	yes yes	[8] [9]
M_3	*Cm* *Cm* *Cm*	SC PWD/SR PWD	33.083 33.1078 33.0577	7.027 7.0355 7.0330	18.499 18.5211 18.5179	90 90 90	94.12 94.137 94.18	90 90 90	yes yes no	[11] [14] [21]
M_3: <M>	*Cm*	SC	12.235	7.073	9.298	90	116.31	90	yes	[12]
M_2	(pOH)	PWD PWD	12.342 12.333	7.143 7.137	25.434 25.442	90	90	90	no no	[1] [3]
M_1	(pOH) *Pc*	PWD PWD	12.332 27.8736	7.142 7.0590	25.420 12.2575	90 90	89.85 116.030	90 90	no no	[1] [20]
T_3 T_3: <T>	(pOH) $P\bar{1}$	PWD PWD/SR	24.633 11.6389	14.290 14.1716	25.412 13.6434	90.06 104.982	89.86 94.622	89.91 90.107	no yes	[1] [17]
T_2 T_2: <T>	(pOH) $P\bar{1}$	PWD PWD/SR	24.528 11.7417	14.270 14.2785	25.298 13.7732	89.98 105.129	89.75 94.415	89.82 89.889	no yes	[1] [16]
T_1	(pOH)	PWD	24.398	14.212	25.103	89.91	89.69	89.69	no	[1]
<T>	$P\bar{1}$	SC	11.67	14.24	13.72	105.5	94.33	90.0	yes	[7]

Table 2. Unit cell parameters used in our study, with both conventional and unconventional unit cells. For the T_1 structure the intermediate unit cells used to pass from the original unit cell of Golovastikov *et al.* [7] to our 3<T> and <T> averaged unit cells are given. To obtain the averaged unit cells <M> of the Nishi and Mumme data (*Cm* space group) [11,12], reverted **a** and **c** axes are used. The - powder - data of Bigaré *et al.* are given in pseudo-orthohexagonal axes.

Unit cell	a (Å)	b (Å)	c (Å)	α (°)	β (°)	γ (°)	V (Å^3)	Space group
$T_1 \equiv G$	11.67	14.24	13.72	105.50	94.33	90	2190	$P\bar{1}$
G'	18.41	14.24	17.33	102.22	76.98	39.34	2190	$P\bar{1}$
Choice 1: 3G'$^{(1)}$	18.41	21.14	17.33	90.03	76.98	89.66	6570	$P\bar{1}$
Choice 2: 3G'$^{(2)}$	27.98	21.14	18.41	89.66	142.89	90.21	6570	$P\bar{1}$
3G' ≡ 9<T>	27.98	21.14	18.41	90.34	142.89	89.79	6570	$P\bar{1}$
3<T>	27.98	7.04	18.41	90.34	142.89	89.79	2190	$P\bar{1}$
<T>	9.33	7.047	18.41	90.34	142.89	89.79	730	$P\bar{1}$
<M>	9.33	7.047	12.33	90.34	115.72	89.79	730	$P\bar{1}$
Choice 1: $M_{3\ Nishi}$	33.083	7.027	18.499	90	94.12	90	4289.4	*Cm*
Choice 3: $M'_{3\ Nishi}$	18.499	7.027	36.725	90	116.04	90	4289.4	*Im*
$<M>_{Nishi}$	9.250	7.027	12.242	90	116.04	90	715.0	*Am*
$<M>_{Mumme}$	9.298	7.073	12.235	90	116.31	90	721.3	*Am*
Choice 1: $M_{1\ Bigaré}$	12.332	7.142	25.420	90	89.85	90	2238.8	*?*
Choice 2: $M'_{1\ Bigaré}$	28.282	7.142	12.332	90	116.0	90	2238.8	*?*
$<M>_{Bigaré}$	9.427	7.142	12.332	90	116.0	90	746.3	*?*

Table 3. Transformation of the idealised coordinates of the Si ions. Si_1', Si_2' and Si_3' are related to Si_1, Si_2 and Si_3 by the inversion centres. $P_{<T>\leftrightarrow<M>}$ is the transformation matrix.

Unit cell	**<T>**			$\mathbf{P_{<T>\leftrightarrow<M>}}$	**<M>**		
	x	y	z		x	y	z
Si_1	1/4	1/4	1/4		0	1/4	1/4
Si_2	1/8	1/4	1/2		5/8 (~2/3)	1/4	1/2
Si_3	3/8	1/4	0		3/8 (~1/3)	1/4	0
Si_1'	3/4	3/4	3/4		0	3/4	3/4
Si_2'	7/8	3/4	1/2		1/3	3/4	1/2
Si_3'	5/8	3/4	0		2/3	3/4	0

Table 4. Effect of the glide mirror c (x,-y,z+1/2) on the idealised coordinates of the Si ions in the <M> unit cell. (see also Table 3 of ref [19]).

Si_1	0	1/4	1/4	→	Si_1'	0	3/4	3/4
Si_2	2/3	1/4	1/2	**c**	Si_2'	1/3	3/4	1/2
Si_3	1/3	1/4	0	→	Si_3'	2/3	3/4	0

Table 5. Results of the Rietveld refinements for M_1-alite data, in the angular range 10-80° ($2\theta_{Cu}$).

Model		**3<M> *Pc***	**3<T> *Pn***	**3<T> *Pm***	**3<M> *Pm***	**3<M> *Am***	**3<T> *Im***
Cell parameters	a(Å)	27.8738(20)	27.8737(19)	27.8743(23)	27.8756(28)	27.8801(29)	27.8750(33)
	b(Å)	7.0591(5)	7.0602(5)	7.0598(5)	7.0618(6)	7.0631(6)	7.0610(8)
	c(Å)	12.2578(8)	18.3439(14)	18.3458(17)	12.2583(12)	12.2611(13)	18.3479(25)
	α (°)	90	90	90	90	90	90
	β (°)	116.031(6)	143.106(4)	143.110(4)	116.022(8)	116.021(9)	143.101(6)
	γ (°)	90	90	90	90	90	90
Shape function	η	0.845(20)	0.857(21)	0.900(28)	0.872(30)	0.877(33)	0.878(41)
	U	0.089(24)	0.130(25)	0.118(29)	0.287(40)	0.186(38)	0.133(46)
	V	-0.044(19)	-0.081(20)	-0.088(24)	-0.246(33)	-0.151(31)	-0.104(39)
	W	0.024(3)	0.031(4)	0.034(5)	0.067(7)	0.048(6)	0.038(8)
	FWHM(°)	0.173	0.175	0.160	0.166	0.165	0.158
Agreement	R_p	16.3	16.0	20.6	23.3	26.6	32.4
Factors	R_{wp}	19.1	18.8	23.8	27.0	29.4	35.6
	R_B	9.2	9.4	15.2	17.4	18.5	27.4
	R_F	8.0	6.8	9.1	11.3	15.1	16.5
	χ^2	8.2	8.2	13.0	17.2	18.4	26.8

Table 6. Refined atomic parameters within the 3<M> *Pc* model.
Unit cell parameters : a, b, c = 27.87438(20), 7.0591(5), 12.2578(8) Å; β = 116.031(6)°.

Atom	x	y	z	Atom	x	y	Z
Ca1	0.0080	0.9825	0.4960	Si2	0.2182	0.2391	0.4704
Ca2	0.8952	0.0054	0.7136	O14	0.1536	0.2538	0.4041
Ca3	0.1110	0.9787	0.2546	O15	0.2432	0.3952	0.4130
Ca4	0.2244	0.0045	0.7376	O16	0.2396	0.2782	0.6144
Ca5	0.3395	0.0092	0.5037	O17	0.2362	0.0291	0.4500
Ca6	0.6731	0.9893	0.5042	Si3	0.1209	0.2593	0.0637
Ca7	0.4507	0.9790	0.2594	O18	0.0903	0.4555	0.0608
Ca8	0.5530	0.9868	0.7118	O19	0.1143	0.2114	-0.0714
Ca9	0.7811	0.0022	0.2620	O20	0.0955	0.0892	0.1102
Ca10	0.8981	0.2812	0.9711	O21	0.1837	0.2811	0.1554
Ca11	0.0114	0.2257	0.7322	Si4	0.3303	0.2352	0.2473
Ca12	0.1088	0.2693	0.5261	O22	0.2663	0.2025	0.1772
Ca13	0.2272	0.2779	0.9564	O23	0.3607	0.0487	0.2322
Ca14	0.3346	0.2696	0.7477	O24	0.3476	0.2729	0.3900
Ca15	0.4419	0.2841	0.5324	O25	0.3464	0.4167	0.1896
Ca16	0.5570	0.2712	0.9720	Si5	0.5484	0.2284	0.4510
Ca17	0.6711	0.2364	0.7493	O26	0.4838	0.2260	0.3922
Ca18	0.7796	0.2465	0.5231	O27	0.5694	0.0342	0.4160
Ca19	0.0040	0.4962	0.0085	O28	0.5726	0.2453	0.5973
Ca20	0.7811	0.5225	0.2519	O29	0.5680	0.4079	0.3986
Ca21	0.8913	0.4809	0.7179	Si6	0.4343	0.2469	-0.0022
Ca22	0.1045	0.5096	0.2864	O30	0.3717	0.2981	-0.0800
Ca23	0.2272	0.5270	0.2235	O31	0.4654	0.2801	-0.0853
Ca24	0.3356	0.4923	0.0115	O32	0.4402	0.0274	0.0402
Ca25	0.6642	0.5020	0.5098	O33	0.4599	0.3822	0.1165
Ca26	0.5579	0.4572	0.7260	Si7	0.6607	0.2607	0.2591
Ca27	0.4400	0.5219	0.2733	O34	0.6040	0.3632	0.1790
O1	0.0342	0.2523	0.6476	O35	0.6669	0.0781	0.1863
O2	0.9628	0.2276	0.8798	O36	0.6631	0.1932	0.3877
O3	0.8481	0.2655	0.7560	O37	0.7089	0.4084	0.2834
O4	0.1588	0.2790	0.7622	Si8	0.8829	0.2503	0.4664
O5	0.3509	0.2198	0.6501	O38	0.8183	0.2552	0.4074
O6	0.2684	0.2624	0.8770	O39	0.9037	0.4098	0.4022
O7	0.6316	0.2560	0.8640	O40	0.9073	0.2930	0.6106
O8	0.7106	0.2694	0.5913	O41	0.9024	0.0431	0.4453
O9	0.5120	0.2657	0.7533	Si9	0.7856	0.2483	0.0219

Si1	0.0049	0.2395	0.2612	O42	0.7531	0.4285	0.0373
O10	-0.0218	0.0818	0.1555	O43	0.7799	0.2433	-0.1154
O11	0.0083	0.4401	0.2007	O44	0.7614	0.0550	0.0488
O12	-0.0312	0.2638	0.3337	O45	0.8481	0.2665	0.1170
O13	0.0645	0.1722	0.3547				

Table 7. Refined atomic parameters within the 3<T> *Pn* model
Unit cell parameters : a, b, c = 27.8737(19), 7.0602(5), 18.3439(14) Å; β = 143.106(4)°.

Atom	x	y	z	Atom	x	y	z
Ca1	0.0189	0.9830	0.0153	Si2	0.7580	0.2629	0.2503
Ca2	0.1745	0.9790	0.4872	O14	0.6637	0.2183	0.1454
Ca3	0.1376	0.0263	0.7130	O15	0.7690	0.4605	0.2199
Ca4	0.97780	0.9977	0.2187	O16	0.7996	0.2799	0.3803
Ca5	0.3734	0.0340	0.7467	O17	0.7998	0.0930	0.2555
Ca6	0.2154	0.0296	0.2732	Si3	0.1197	0.2458	0.0177
Ca7	0.3015	0.9891	0.2228	O18	0.0450	0.2834	0.9811
Ca8	0.3367	0.9606	-0.0163	O19	0.0927	0.2880	0.9016
Ca9	0.5358	0.9868	0.2492	O20	0.1482	0.0272	0.0594
Ca10	0.2182	0.2746	0.9566	O21	0.1930	0.3846	0.1286
Ca11	0.5612	0.2670	0.9672	Si4	0.4718	0.2477	0.0335
Ca12	0.2634	0.2171	0.7415	O22	0.4617	0.0453	0.0617
Ca13	0.5908	0.2494	0.7328	O23	0.4016	0.2729	-0.1119
Ca14	0.2911	0.2654	0.5251	O24	0.4660	0.4166	0.0859
Ca15	0.6235	0.2716	0.5282	O25	0.5580	0.2559	0.0982
Ca16	0.8931	0.2608	0.9607	Si5	0.0472	0.2353	0.4687
Ca17	0.9214	0.2540	0.7379	O26	-0.0394	0.2066	0.4015
Ca18	0.9624	0.2960	0.5286	O27	0.0440	0.4160	0.4104
Ca19	0.0133	0.4979	0.0038	O28	0.1140	0.2715	0.6123
Ca20	0.1745	0.5035	0.4976	O29	0.0701	0.0471	0.4506
Ca21	0.0371	0.5035	0.7556	Si6	0.7105	0.2475	0.4634
Ca22	0.8709	0.5138	0.25431	O30	0.6273	0.2560	0.4073
Ca23	0.1390	0.4720	0.7184	O31	0.7189	0.0426	0.4347
Ca24	0.9705	0.5212	0.2180	O32	0.7846	0.2790	0.6090
Ca25	0.2138	0.5163	0.2893	O33	0.7111	0.4124	0.4028
Ca26	0.3060	0.5287	0.2258	Si7	0.0839	0.2786	0.2426
Ca27	0.3439	0.4758	0.0122	O34	0.9977	0.3625	0.1617
O1	0.5924	0.2380	0.6493	O35	0.0845	0.2400	0.1562
O2	0.2509	0.2650	0.6478	O36	0.1004	0.0819	0.3055
O3	0.5859	0.2357	0.8661	O37	0.1531	0.4302	0.3470
O4	0.2585	0.2592	0.8779	Si8	0.7992	0.2459	0.0293
O5	0.0994	0.2535	0.7598	O38	0.7329	0.3903	0.9814
O6	0.4349	0.2570	0.7435	O39	0.7772	0.1953	0.9189
O7	0.7479	0.2775	0.7619	O40	0.8000	0.0534	0.0784
O8	0.9182	0.2215	0.6541	O41	0.8865	0.3445	0.1386
O9	0.8891	0.2672	0.8552	Si9	0.3937	0.2219	0.4942
Si1	0.4126	0.2397	0.2514	O42	0.3089	0.3289	0.4017
O10	0.3188	0.2139	0.1568	O43	0.3862	0.0677	0.4201
O11	0.4281	0.1766	0.1866	O44	0.4179	0.1155	0.5987
O12	0.4658	0.1087	0.3699	O45	0.4620	0.3757	0.5565
O13	0.4377	0.4597	0.2923				